Supporting information for:

Bimetallic hexanuclear clusters in Ce/Zr-UiO-66 MOFs: *in situ* FTIR spectroscopy and modelling insights

Cesare Atzori*,[a] Kirill A. Lomachenko,[b] Jannick Jacobsen,[c] Norbert Stock,[c] Alessandro Damin,[a] Francesca Bonino,[a] Silvia Bordiga[a]

[a] Department of Chemistry, NIS and INSTM Reference Centre, Università di Torino, Via G. Quarello 15, I-10135 and Via P. Giuria 7, I-10125 Torino, Italy
[b] European Synchrotron Radiation Facility, 71 Avenue des Martyrs, CS 40220, 38043 Grenoble Cedex 9, France
[c] Institut für Anorganische Chemie, Christian-Albrechts-Universität zu Kiel, Max-Eyth-Straße 2, 24118 Kiel, Germany

*Corresponding author e-mail: cesare.atzori@unito.it

Outline:

1. Details about calculations in the Three Cluster Model (TCM)

The relative concentrations (i.e. the probability to encounter such a stoichiometry) of Ce_6, $CeZr_5$ and Zr_6 clusters, the only clusters expected in the TCM hypothesis, as a function of the total Ce content (in molar fraction, $0 < \chi_{Ce} < 1$, $\chi_{Ce} = {Ce}/{Ce + Zr}$) of the material were calculated using the following equations:

$$\begin{cases} P_{Ce_6}(\chi_{Ce}) = 1 - 6 \cdot \chi_{Ce} \; for \; \chi_{Ce} \leq \frac{1}{6}, 0 \; elsewhere \\ P_{CeZr_5}(\chi_{Ce}) = 1 - P_{Ce_6} \; for \; \chi_{Ce} \leq \frac{1}{6}, 1 - P_{Zr_6} \; elsewhere \\ P_{Zr_6}(\chi_{Ce}) = 0 \; for \; \chi_{Ce} \leq \frac{1}{6}, \left(\chi_{Ce} - \frac{1}{6}\right) * \frac{6}{5} \; elsewhere \end{cases}$$

Cluster with other stoichometries, (e.g. Ce_2Zr_4) are kept at zero concentration as expected for the TCM model. The concentrations of having every kind of cluster sums up to 1, supporting the correctness of the equations.

Table S1 – Cluster abundancies calculated with the Three Cluster Model (TCM) of the samples used in the present work.

Sample	Three Cluster Model (TCM)						
	Cluster abundance (%)						
	Zr_6	$CeZr_5$	Ce_2Zr4	Ce_3Zr_3	Ce_4Zr_2	Ce_5Zr	Ce_6
Zr-UiO-66	100	0	0	0	0	0	0
Ce5	69.9	30.1	0	0	0	0	0
Ce10	39.8	60.2	0	0	0	0	0
Ce14	15.7	84.3	0	0	0	0	0
Ce33	0	80.3	0	0	0	0	19.7
Ce58	0	50.4	0	0	0	0	49.6
Ce79	0	25.2	0	0	0	0	74.8
Ce-UiO-66	0	0	0	0	0	0	100

2. Details about combinatorial calculations in the Multi Cluster Model (MCM)

The relative concentrations of every Ce_xZr_{6-x} cluster as a function of the total Ce content (in molar fraction, $0 < \chi_{Ce} < 1$) of the material were calculated considering the different number of *x* Ce atoms that can be chosen from a 6-element set (i.e. the x-combinations) and the probability to have that particular combination of Ce and Zr atoms. The abundances have been calculated using the following formula:

$$P_{Ce_xZr_{6-x}}(\chi_{Ce}) = \binom{6}{x} \cdot {\chi_{Ce}}^x \cdot (1-\chi_{Ce})^{6-x}$$

Where $P_{Ce_xZr_{6-x}}$ is the probability to have a cluster with *x* Ce atoms and χ_{Ce} is the Ce molar fraction in respect to the total metal content of the MOF, $\chi_{Ce} = {Ce}/{Ce + Zr}$.

Also in this case the probability of having every kind of cluster does sum up to 1, supporting the correctness of the formula.

Table S2 – Cluster abundancies calculated with the Multi Cluster Model (MCM) of the samples used in the present work. Concentrations below 0.01% are represented as "~0" for the sake of clarity.

Sample	Multi Cluster Model (MCM)						
	Cluster abundance (%)						
	Zr_6	$CeZr_5$	Ce_2Zr4	Ce_3Zr_3	Ce_4Zr_2	Ce_5Zr	Ce_6
Zr-UiO-66	100	0	0	0	0	0	0
Ce5	73.5	23.2	3.05	0.21	~0	~0	~0
Ce10	53.1	35.4	9.84	1.46	0.12	~0	~0
Ce14	40.5	39.5	16.1	3.49	0.43	0.02	~0
Ce33	9.05	26.7	32.9	21.6	7.99	1.57	0.13
Ce58	0.55	4.55	15.7	28.9	29.9	16.5	3.81
Ce79	0.01	0.19	1.82	9.13	25.8	38.8	24.3
Ce-UiO-66	0	0	0	0	0	0	100

3. Synthesis

Cerium (IV) ammonium nitrate (98 %, $(NH_4Ce(NO_3)_6$, CAN, Alfa Aesar), 1,4-benzenedicarboxylic acid (98 %, H_2BDC, Sigma-Aldrich), zirconyl nitrate monohydrate ($ZrO(NO_3)_2 \cdot H_2O$, ABCR), zirconium (IV) chloride (99 %, $ZrCl_4$, Sigma-Aldrich), N,N-dimethylformamide (99 %, DMF, Grüssing GmbH) and formic acid (100 %, HCOOH, BASF) were used as obtained.

The synthesis of the six mixed-metal Ce/Zr-UiO-66 compounds was carried out as previously reported,[1] using Pyrex glass reaction tubes (reaction volume 7 mL). The linker 1,4-benzenedicarboxylic acid (H_2BDC, 63.8 mg) was dissolved in N,N-dimethylformamide (DMF, 1.8 mL) and transferred into the glass reactor. Subsequently the formic acid (HCOOH, 515 µL) and finally the aqueous solutions of CAN (0.533 mol/L) and $ZrO(NO_3)_2 \cdot H_2O$ (0.533 mol/L) were added in the desired stoichiometry (Table S3). The total volume of the two metal salt solutions was always 600 µL.

Table S3 – Parameters for the synthesis of pure Ce-UiO-66 and mixed-metal Ce/Zr UiO-66 samples. Ce, Zr, H_2BDC and HCOOH values are intended as mutual molar ratios.

Sample	**Molar ratio**				**Ce**	**Zr**	**H_2BDC**	**DMF**	**HCOOH**
	Ce	Zr	H_2BDC	HCOOH	[µL]	[µL]	[mg]	[mL]	[µL]
Ce5	0.15	2.85	3.6	128	30	570	63.8	1.8	515
Ce10	0.3	2.7	3.6	128	60	540	63.8	1.8	515
Ce14	0.5	2.5	3.6	128	100	500	63.8	1.8	515
Ce33	1.5	1.5	3.6	128	300	300	63.8	1.8	515
Ce58	2.25	0.75	3.6	128	450	150	63.8	1.8	515
Ce79	2.75	0.25	3.6	128	550	50	63.8	1.8	515
Ce-UiO-66	3.0	0.0	3.6	128	600	0	63.8	1.8	515

Zr-UiO-66 was synthesized following the procedure reported by Cavka et al..[2] Zirconium (IV) chloride (530 mg) and 1,4-benzenedicarboxylic acid (H_2BDC, 340 mg) were dissolved in N,N-dimethylformamide (DMF, 20 mL). This mixture was sealed in a steel autoclave and placed in an oven at 120°C for 24 hours. After the synthesis the solvothermal reactor was cooled down to room temperature and the precipitate was centrifuged. The mother liquor was decanted off and the product was re-dispersed and centrifuged two times in DMF (5 mL) and three times in acetone (5 mL). Finally, the MOF was dried in air at 70°C.

4. EDX spectroscopy

Table S4 – Result of the EDX measurements on the mixed-metal Ce/Zr-UiO-66 compounds.

Sample	Ce content, at %	Standard deviation, at %
Ce5	5.2	0.9
Ce10	9.9	0.2
Ce14	13.8	0.2
Ce33	33.4	1.2
Ce58	58.1	0.6
Ce79	78.9	1.3

5. μ_3-OH abundancies in TCM and MCM

In order to compute the different OH abundances, in terms of neighbouring atoms, from the cluster concentrations the abundancies from the two models (TCM and MCM) have been multiplied for the following coefficients in Table S5, which have been obtained simply counting the different kinds of μ_3-OH present in every Ce_xZr_{6-x} cluster with the help of the molecular graphics software MOLDRAW[3] and the CONFCNT[4] function of the CRYSTAL[5] package. The crystallographic restraint of having 4 OHs arranged to form a tetrahedron within the octahedral hexanuclear cluster, as previously published by Valenzano et al.[6] and Øien-Ødegaard et al.[7] was taken into account.

The non-integer number of OHs present in Ce_4Zr_2, Ce_3Zr_3, Ce_2Zr_4 clusters is due to account for different modes of building hexanuclear clusters with 2 to 3 substituent atoms and thus having different OHs.

Table S5 – Different kinds of μ_3-OH groups, in terms of neighbouring atoms, present in every mixed-metal cluster.

μ_3-OH	Clusters						
	Zr_6	$CeZr_5$	Ce_2Zr_4	Ce_3Zr_3	Ce_4Zr_2	Ce_5Zr	Ce_6
Zr_3	4	2	0.8	0.4	0	0	0
$CeZr_2$	0	2	2.4	1.6	0.8	0	0
Ce_2Zr	0	0	0.8	1.6	2.4	2	0
Ce_3	0	0	0	0.4	0.8	2	4

The abundancies of different μ_3-OH were calculated multiplying (i.e. a matrix multiplication) the coefficients in Table S5 with the concentrations reported in Tables S3 and S4 for respectively the TCM and MCM.

Table S6 – μ_3-OH abundancies calculated within the TCM and the MCM.

Sample	Three Cluster Model (TCM)				Multi Cluster Model (MCM)			
	(μ_3-OH) abundance (%)				**(μ_3-OH) abundance (%)**			
	Zr_3	$CeZr_2$	Ce_2Zr	Ce_3	Zr_3	$CeZr_2$	Ce_2Zr	Ce_3
Zr-UiO-66	100	0	0	0	100	0	0	0
Ce5	85	15	0	0	85.7	13.5	0.71	0.01
Ce10	70	30	0	0	72.9	24.3	2.7	0.1
Ce14	58	42	0	0	63.6	31.1	5.06	0.27
Ce33	40.2	40.2	0	19.6	30.1	44.4	21.9	3.59
Ce58	25.2	25.2	0	49.6	7.41	30.7	42.4	19.5
Ce79	37.6	37.6	0	74.8	0.93	10.4	39.3	49.3
Ce-UiO-66	0	0	0	100	0	0	0	100

6. Details about DFT calculations

Periodic DFT[8] based calculations were performed by exploiting the hybrid B3LYP[9,10] functional and the empirical D3(BJ)[11–13] scheme for the description of dispersive interactions and including the Axilrod-Teller-Muto type three-body term. In the whole set of calculations, the CRYSTAL software[5,14] package was employed: this allows a complete treatment of periodic systems through the use of atom-centred linear combinations of Gaussian type functions for the description of atomic orbitals (basis set). Basis set adopted in present calculations is below described:

a) Hay-Wadt small-core pseudopotentials (SC-ECP) were used to describe the first 28 Zr inner electrons. The remaining 8 electrons were treated explicitly using a [4sp3d1f] basis set. The same scheme was already exploited by Sophia et al.[15] to study Zr-containing perovskites. See also http://www.crystal.unito.it/basis-sets.php.

b) Ce inner electrons (28) were replaced by an effective core potential (ECP), the remaining 30 electrons being explicitly treated through a (10sp7d8f)/[4sp2d3f] basis set. The same scheme was already employed in Ref[16] for Ce description in CeO_2 and Ce_2O_3 systems. See also http://www.crystal.unito.it/basis-sets.php.

c) O and C atoms were described through a (8s6sp2d)/[1s3sp2d] and (6s5sp2d)/[1s3sp2d] all-electron basis sets respectively. They were obtained by ones employed in Ref[6], simply by splitting the original d shell through an even tempered recipe.

d) For H atoms the adopted all electron basis set was a (7s1p)/[3s1p]] one already adopted in Ref[17]. See also http://www.crystal.unito.it/basis-sets.php.

Numerical accuracy in energy calculation were determined by setting thresholds for mono- and bi-electronic integral to {1188836} through the keyword (TOLINTEG). Shrinking factor parameter (keyword SHRINK), determining the k-points sampling in the reciprocal space, was set to 3 (corresponding to 4 irreducible k points). The defaults values for all the unreported computational parameters concerning the structure optimization, frequency and the associated IR intensities calculation were used.

Vibrational modes were calculated within the harmonic approximation at the Γ point using the FREQCALC[14] keyword embedded in CRYSTAL. A scaling factor of 0.959 (chosen in order to align the (μ_3-OH)Zr_3 band at 3674 cm^{-1}) was applied to the calculated wavenumbers to allow a direct comparison with the experimental adsorption bands. IR intensities were calculated through the CPHF/CPKS (Coupled-Perturbed Hartree–Fock/Kohn–Sham) approach as implemented in the INTCPHF keyword.

Calculated spectra, as reported in Figures 2a and S1, were obtained simply placing a gaussian curve with a FWHM of 6 cm^{-1} at the scaled wavenumbers, the width of the peaks was chosen in order to account for the experimental broadening of the bands and facilitate the reading of the spectra.

7. Experimental details about FTIR measurements

All FTIR spectra were recorded at 2 cm^{-1} resolution on a Bruker Vertex 70 spectrophotometer equipped with an MCT detector cooled at the liquid nitrogen temperature. A quartz cell equipped with KBr windows of local construction was used in order to keep the controlled atmosphere and allow for the dosage of CD_3CN vapours in an in-situ manner. All samples were prepared in the form of thin self-supporting pellets which were outgassed in dynamic high vacuum ($5 \cdot 10^{-4}$ mbar) at temperatures varying from 100°C to 180°C for durations varying from 4 to 16 hours depending on the Ce/Zr ratio. Details about the activation procedure for every sample are reported in Table S7. The necessity for different thermal treatments for every sample is due to the different thermal stability and tendency to cluster dehydroxylation with respect to the Ce/Zr ratio[1,6,18] and the necessity to have a MOF sufficiently desolvated but still having all the expected OH moieties.

Table S7 – Thermal treatment conditions for Zr-UiO-66, Ce-UiO-66 and mixed Ce/Zr-UiO-66 samples prior to FTIR measurements.

Sample	Temperature	Time
Zr-UiO-66	180°C	4 h
Ce5	150°C	16 h
Ce10	150°C	16 h
Ce14	150°C	16 h
Ce27	120°C	16 h
Ce66	100°C	16 h
Ce79	100°C	16 h
Ce-UiO-66	100°C	4 h

.

8. Linear combinations of simulated vibrational spectra

The linear combinations of the v(OH) bands in the spectra of TCM and MCM (Figure 3a and 3c of the main text) are calculated starting from the values presented in Figure 2a using the following equation.

$$A_{tot}(\lambda) = a \cdot A_{Zr3}(\lambda) + b \cdot A_{CeZr2}(\lambda) + c \cdot A_{Ce2Zr}(\lambda) + d \cdot A_{Ce3}(\lambda)$$

A_{tot} is the total absorbance and A_{Ce3}, A_{Ce2Zr}, A_{CeZr2} and A_{CeZr2} are the calculated absorbances of the stretching bands as plotted in Figure 2a. The variables a, b, c and d are the coefficients plotted in Figure 1c in the main text and reported in Table S6 respectively for (μ_3-OH)Zr_3, (μ_3-OH)$CeZr_2$, (μ_3-OH)Ce_2Zr and (μ_3-OH)Ce_3.

For the sake of clarity, Figure 1 in the main text, shows the percentage of the total metal content and not the molar ratio. One can simply multiply the molar ratio by 100 in order to apply these equations to percentages.

9. Calculated IR spectra

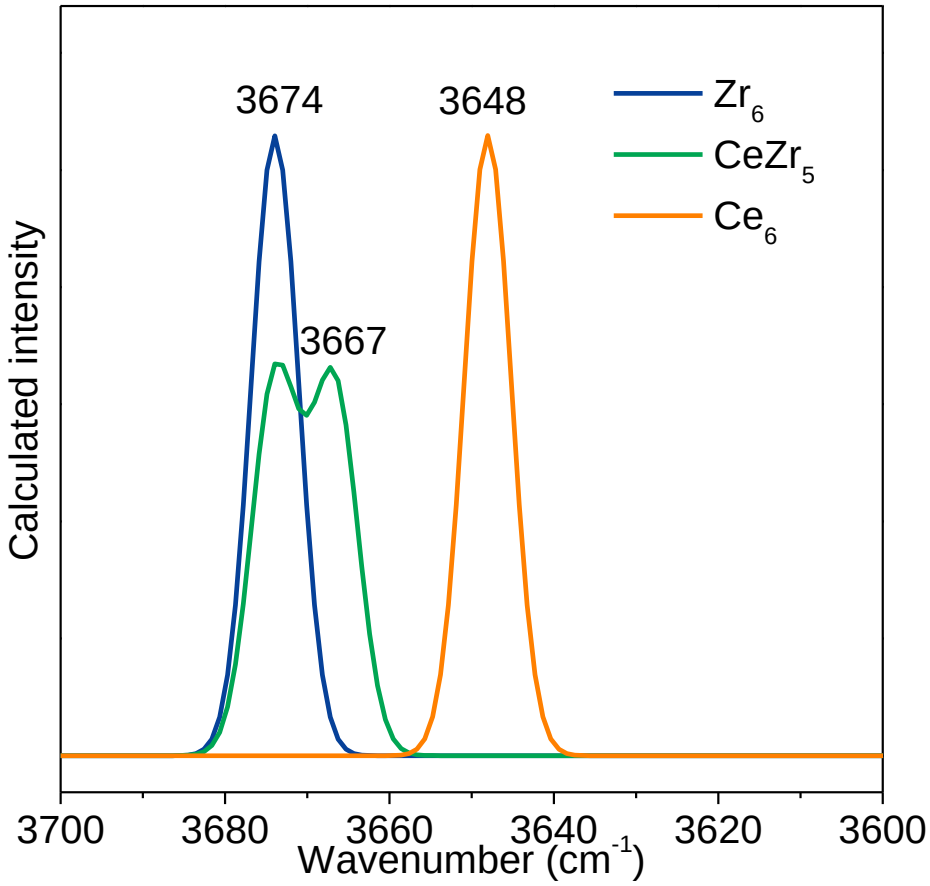

Figure S1 – Calculated IR spectra of the ν(OH) region on Zr_6, $CeZr_5$ and Ce_6 models, respectively in blue, green and orange curves.

Figure S1 reports the spectra calculated from the Ce_6, $CeZr_5$ and Zr_6 crystalline models which shows bands with an almost equal intensity for Zr_6 and Ce_6 clusters. Each $CeZr_5$ cluster, having four μ_3-OH groups, presents only two different types of μ_3-OH groups: those linked to 1 Ce and 2 Zr or 3 Zr. The relative abundance of these two species is 1:1 (two OH groups of each type).

10. In-situ CD_3CN dosage FTIR experiments

Acetonitrile is a small molecule with a high proton affinity and for this reason it is traditionally used as a probe molecule in FTIR experiments. In principle the crystallographic structure of UiO-66 does not take into account the existence of any proper open-metal sites (OMS), otherwise CD_3CN, being a relative strong base, is known to introduce structural changes in the first coordination sphere of the metal cations otherwise inaccessible by weaker probes as CO.[19,20] For this reason the acidity probed in this way should be considered as an induced property and not a readily available acidity: this fact has strong implications in applications such as catalysis.

Deuteration is needed to overcome the well-known Fermi resonance phenomenon that otherwise will complicate the spectra.[19] The ν(CN) mode is perturbed (typically upshifted) upon interaction with acidic sites and the wavenumber of the corresponding band allows to discriminate between different interacting sites. In particular complexes with OH groups are expected in the 2300-2285 cm^{-1} range while with Lewis sites up to 2330 cm^{-1}.[20–22] After the same thermal treatment reported in Table S7, the vapours of CD_3CN at room temperature were admitted into the IR cell already used for recording the spectra reported in Figure S2 (red spectra) and the desorption process, upon pressure reduction inside the cell, was followed taking spectra reported as grey curves until reaching the minimum coverage (green curves).

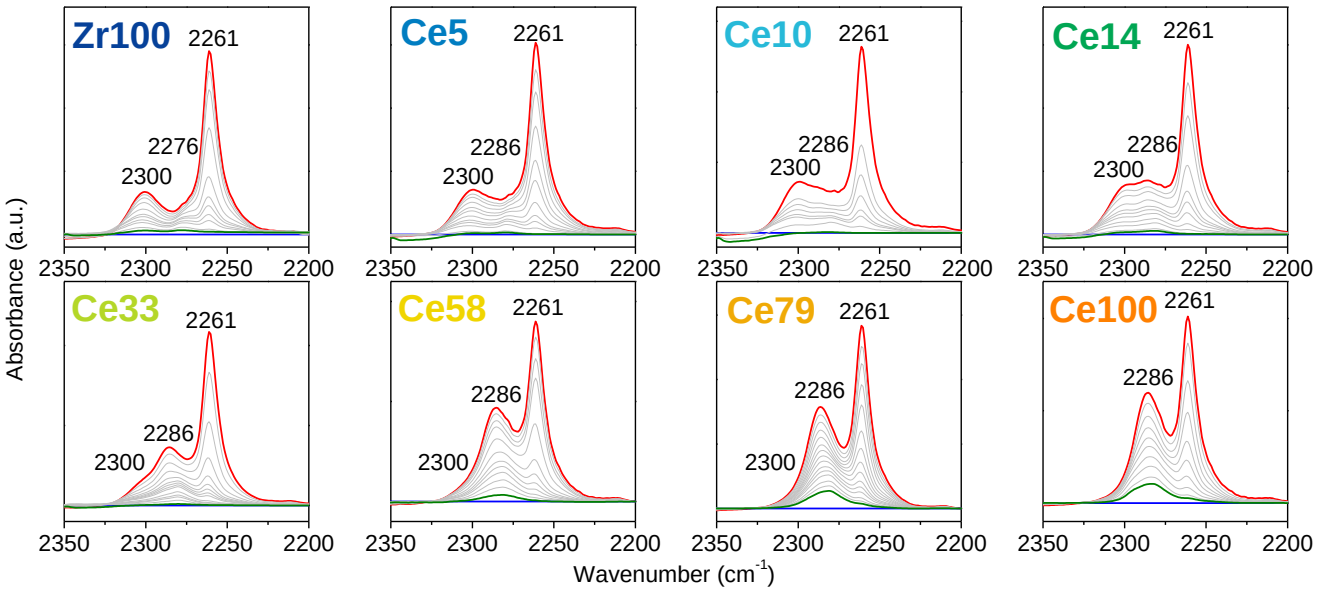

Figure S2 – IR spectra of the background-subtracted ν(CN) stretching zone of CD_3CN dosed on Ce/Zr-UiO-66 samples. Maximum, intermediate and minimum coverages are reported, respectively, in red, grey and green colours being the background drawn as a blue curve.

Figure S2 reports an in situ CD_3CN dosage experiment done for each sample presented in this work. The Zr-UiO-66 sample (Zr100) shows bands at 2300 cm^{-1}, 2276 cm^{-1} and 2261 cm^{-1}, ascribable respectively to the ν(CN)

stretching mode of a $D_3CCN\cdots Zr^{4+}$, $D_3CCN\cdots HO$ adducts and a liquid-like CD_3CN (which is the first one to be desorbed upon outgassing) into the pore system of the material[20,23]. Conversely the pure Ce-UiO-66 spectra, Ce100, differ from Zr100 only for the absence of the band at 2300 cm^{-1} and the presence of a new band at 2286 cm^{-1} readily assignable to a $D_3CCN\cdots Ce^{4+}$ species. The weak feature at 2276 cm^{-1}, still present, is hardly detectable as it is included as a shoulder of the stronger 2286 cm^{-1} band. This last consideration can also be affirmed for the whole mixed Ce/Zr series. In the mixed Ce/Zr samples (Ce5, Ce10, Ce14, Ce33, Ce58 and Ce79) all the features recognized separately for pure Zr (Zr100) and pure Ce (Ce100) are found with different relative intensities. It should be noticed that even upon addition of 14% of Ce the absorbance of the band associated to Ce^{4+} is already higher than the one assigned to Zr^{4+} Lewis acidic sites. This evidence can be explained by two main mechanisms: i) the molar extinction coefficient of the ν(CN) mode associated to the $D_3CCN\cdots Ce^{4+}$ adduct is much higher than the one of $D_3CCN\cdots Zr^{4+}$; ii) the coordination sphere of Ce^{4+} may be more flexible than the one of Zr^{4+} and therefore the abundance of the Ce^{4+} adduct may be higher.[24] This is not surprising as the ionic radii of Ce^{4+} (111 pm) is higher than the one of Zr4+ (98 pm)[25] and therefore we are convinced that the coordination flexibility is the decisive factor that must be taken into account in explaining our spectroscopic findings.

References

1 M. Lammert, C. Glißmann and N. Stock, *Dalt. Trans.*, 2017, **46**, 2425–2429.

2 J. H. Cavka, S. Jakobsen, U. Olsbye, N. Guillou, C. Lamberti, S. Bordiga and K. P. Lillerud, 2008, **6**, 13850–13851.

3 P. Ugliengo, G. Borzani and D. Viterbo, *J. Appl. Crystallogr.*, 1988, **21**, 75.

4 S. Mustapha, P. D'Arco, M. De La Pierre, Y. Noël, M. Ferrabone and R. Dovesi, *J. Phys. Condens. Matter*, 2013, **25**, 105401.

5 R. Dovesi, A. Erba, R. Orlando, C. M. Zicovich-Wilson, B. Civalleri, L. Maschio, M. Rérat, S. Casassa, J. Baima, S. Salustro and B. Kirtman, *Wiley Interdiscip. Rev. Comput. Mol. Sci.*, 2018, **8**, e1360.

6 L. Valenzano, B. Civalleri, S. Chavan, S. Bordiga, M. H. Nilsen, S. Jakobsen, K. P. Lillerud and C. Lamberti, *Chem. Mater.*, 2011, **23**, 1700–1718.

7 S. Øien, D. Wragg, H. Reinsch, S. Svelle, S. Bordiga, C. Lamberti and K. P. Lillerud, *Cryst. Growth Des.*, 2014, **14**, 5370–5372.

8 P. Hohenberg and W. Kohn, *Phys. Rev.*, 1964, **136**, B864–B871.

9 A. D. Becke, *J. Chem. Phys.*, 1993, **98**, 1372–1377.

10 C. Lee, W. Yang and R. G. Parr, *Phys. Rev. B*, 1988, **37**, 785–789.

11 S. Grimme, J. Antony, S. Ehrlich and H. Krieg, *J. Chem. Phys.*, 2010, **132**, 154104.

12 S. Grimme, S. Ehrlich and L. Goerigk, *J. Comput. Chem.*, 2011, **32**, 1456–1465.

13 S. Grimme, A. Hansen, J. G. Brandenburg and C. Bannwarth, *Chem. Rev.*, 2016, **116**, 5105–5154.

14 S. C. R. Dovesi, V.R. Saunders, C. Roetti, R. Orlando, C. M. Zicovich-Wilson, F. Pascale, B. Civalleri, K. Doll, N.M. Harrison, I.J. Bush, Ph. D'Arco, M. Llunel, M. Causà, Y. Noel, L. Maschio, A. Erba, M. Rérat and S.Casassa, CRYSTAL17 User's Manual, 2018.

15 G. Sophia, P. Baranek, C. Sarrazin, M. Rérat and R. Dovesi, *Phase Transitions*, 2013, **86**, 1069–1084.

16 J. Graciani, A. M. Márquez, J. J. Plata, Y. Ortega, N. C. Hernández, A. Meyer, C. M. Zicovich-Wilson and J. F. Sanz, *J. Chem. Theory Comput.*, 2011, **7**, 56–65.

17 R. Dovesi, C. Ermondi, E. Ferrero, C. Pisani and C. Roetti, *Phys. Rev. B*, 1984, **29**, 3591–3600.

18 K. A. Lomachenko, J. Jacobsen, A. L. Bugaev, C. Atzori, F. Bonino, S. Bordiga, N. Stock and C. Lamberti, *J. Am. Chem. Soc.*, 2018, **140**, 17379–17383.

19 F. Bonino, A. Damin, S. Bordiga, C. Lamberti and A. Zecchina, *Langmuir*, 2003, **19**, 2155–2161.

20 K. Chakarova, I. Strauss, M. Mihaylov, N. Drenchev and K. Hadjiivanov, *Microporous Mesoporous Mater.*, 2019, **281**, 110–122.

21 F. Ragon, B. Campo, Q. Yang, C. Martineau, A. D. Wiersum, A. Lago, V. Guillerm, C. Hemsley, J. F. Eubank, M. Vishnuvarthan, F. Taulelle, P. Horcajada, A. Vimont, P. L. Llewellyn, M. Daturi, S. Devautour-Vinot, G. Maurin, C. Serre, T. Devic and G. Clet, *J. Mater. Chem. A*, 2015, **3**, 3294–3309.

22 C. Morterra, M. Peñarroya Mentruit and G. Cerrato, *Phys. Chem. Chem. Phys.*, 2002, **4**, 676–687.

23 F. Nouar, M. I. Breeze, B. C. Campo, A. Vimont, G. Clet, M. Daturi, T. Devic, R. I. Walton and C. Serre, *Chem. Commun.*, 2015, **51**, 14458–14461.

24 J. Jacobsen, B. Achenbach, H. Reinsch, S. Smolders, F. D. Lange, G. Friedrichs, D. De Vos and N. Stock, *Dalt. Trans.*, 2019, **48**, 8433–8441.

25 R. D. Shannon, *Acta Crystallogr. Sect. A*, 1976, **32**, 751–767.